

# Fast Bayesian Uncertainty Estimation of Batch Normalized Single Image Super-Resolution Network

Aupendu Kar

Indian Institute of Technology Kharagpur  
Kharagpur, WB, India

aupendukar@iitkgp.ac.in

Prabir Kumar Biswas

Indian Institute of Technology Kharagpur  
Kharagpur, WB, India

pkb@ece.iitkgp.ac.in

## Abstract

*In recent years, deep convolutional neural network (CNN) has achieved unprecedented success in image super-resolution (SR) task. But the black-box nature of the neural network and due to its lack of transparency, it is hard to trust the outcome. In this regards, we introduce a Bayesian approach for uncertainty estimation in super-resolution network. We generate Monte Carlo (MC) samples from a posterior distribution by using batch mean and variance as a stochastic parameter in the batch-normalization layer during test time. Those MC samples not only reconstruct the image from its low-resolution counterpart but also provides a confidence map of reconstruction which will be very impactful for practical use. We also introduce a faster approach for estimating the uncertainty, and it can be useful for real-time applications. We validate our results using standard datasets for performance analysis and also for different domain-specific super-resolution task. We also estimate uncertainty quality using standard statistical metrics and also provides a qualitative evaluation of uncertainty for SR applications.*

## 1. Introduction

Single image super-resolution (SISR) is an ill-posed low vision problem which generates high resolution (HR) image from a low resolution (LR) image. There is a possibility of making an infinite number of HR images which can be sub-sampled into the same LR image. Due to the advancement of deep learning techniques, the community has developed a state-of-the-art SISR network using deep neural architectures [38]. SR has a wide range of applications from surveillance and security [44] to medical imaging [30] and many more. Other than improving the perceptual quality of images for human interpretation, SISR helps to boost the performance of different automated machine learning or computer vision task [29].

Uncertainty is a powerful tool for any prediction and reconstruction system. The confidence of the system's output will help to improve the decision-making process. It is a useful tool for any computer vision problem. We use the concept of uncertainty for image super-resolution. Deep learning based SISR techniques learns features from a dataset and features are dependent on the images of the dataset. But real-world pictures are completely different and contain more complex textures than the training set. Unseen texture during test time can create inappropriate reconstruction. Due to the black-box nature of deep learning models, it is almost impossible to know the limitation of models or trustability of reconstructed SR image which is further processed to other computer vision task. But we have witnessed that some artifacts, blurriness or distortions in an image can significantly degrade the performance of deep learning based models [22]. Some deformation in reconstructing LR facial image may lead to wrong output in a recognition system or any deformed reconstruction in tumor image may lead to the incorrect estimation of tumor size. Uncertainty in deep learning (DL) models have a transparent and robust effect in DL-based computer vision task.

Bayesian approaches in super-resolution not only provides the reconstructed HR image but also provides the posterior distribution of super-resolution. Recent progress in Bayesian deep learning approaches uses Monte Carlo samples that come from a posterior distribution via dropout [32] or batch-normalization [13]. Dropout during test time or stochastic batch mean-variance during testing helps to generate MC samples [8, 33]. Monte Carlo methods for deep learning model uncertainty estimation is successfully applied to classification, segmentation [16, 27], camera relocalization [17] problems. Generally, the deep learning community does not use dropout in image reconstruction applications, but batch normalization is most common in SISR, denoising, etc. Therefore, we use batch-normalization uncertainty to analyze SISR uncertainty.

In this article, we propose a Bayesian approach to measure the quality of reconstructed HR images from down-

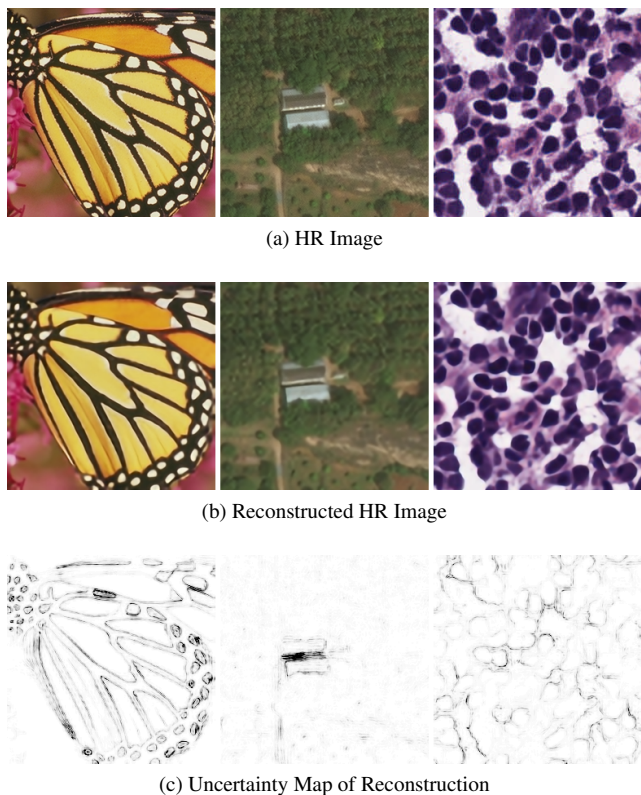


Figure 1: This example shows the performance of the Bayesian approach in SISR. The first image from the left side is from 'Set5' dataset; the middle one is a satellite [1] image and the last one is a histopathology [21] image. The reconstructed image is with scaling factor  $\times 4$ . We generate uncertainty map and reconstruct HR image using 25 MC samples. We observe model uncertainty in edges and geometrically complex regions like boundaries of nuclei in histopathology sample, and the gap between two buildings in the satellite image. We use the model trained on natural images to reconstruct the HR images of those different domain data without any domain adaptation.

sampled LR images. For this purpose, we add widely used batch-normalization layer in the super-resolution network, and it helps to generate Monte Carlo (MC) samples. These samples are different possible HR images from a single LR image. We use the mean of those HR images to get the reconstruction, and the variation between those HR images gives an idea about the uncertainty of reconstruction. We estimate the uncertainty of the reconstruction from those MC samples. We measure the quality of uncertainty using standard statistical metrics and observe the relation between reconstruction quality and uncertainty. We also propose a faster approach for generating MC samples and this faster approach can be extended to any other computer vision applications. In our method, we got MC samples in a single

feed-forward, and due to this, it is useful in real-time applications.

Our contributions in this paper are as follows:

1. We use the standard approach of uncertainty estimation of DL models using batch-normalization. Our work proposes a better and faster strategy for uncertainty estimation and overcame the hurdle of variable image size. Our procedure generates any number of MC samples in a single shot.
2. We have demonstrated a Bayesian uncertainty estimation approach for SISR, and as of our knowledge, we are the first one to estimate uncertainty in deep learning based image reconstruction.
3. We use Monte Carlo batch-normalization (MCBN) for uncertainty estimation in super-resolution network.
4. We have discussed the advantages of uncertainty in SISR and its applications from medical image to satellite image super-resolution. We also analyzed the uncertainty map and its significance.

## 2. Related Work

### 2.1. Single Image Super-Resolution

SISR has extensive literature due to different studies in the last few decades. Recent advancement of deep learning (DL) methods has achieved significant improvement in that field [5, 18, 36] and different computer vision task [42, 41, 43, 15]. SRCNN [5] first explored the convolutional neural network for establishing a non-linear mapping between interpolated LR images and its HR counterparts. It has achieved superior performance than other example-based methods like nearest neighbor [6], sparse representation [39], neighborhood embedding [34], etc. VDSR [18] proposed a deeper architecture and showed performance improves with the increase of network depth and converge faster using residual learning. After that different DL based approaches [19, 23, 43, 24] have been proposed and achieved state-of-the-art performance in the standard dataset. In our work, we used VDSR [18] architecture for uncertainty analysis as it is the first deep architecture for SISR.

### 2.2. Bayesian Uncertainty

Bayesian models are generally used to model uncertainty, and different approaches have been developed to adapt NNs to Bayesian reasoning like placing a prior distribution over parameters. Due to difficult in inferencing [7] of Bayesian neural networks (BNNs), some approaches [8, 33] have been taken to approximate BNNs. Bayesian deep learning approaches utilized MC samples generated via dropout [32] or batch normalization [13] to approximate posterior distribution. Dropout [32] can be treated as approximate Bayesian model as multiple predictions

through trained model by sampling predictions using different dropout mask, and In case of batch-normalization [13], stochastic parameters batch mean and batch variance are used to generate multiple predictions. [33] shows batch-normalized neural network can be approximated to the Bayesian model. We use a batch-normalized neural network for SISR as it is widely used in image reconstruction applications.

### 3. Proposed Method

We propose a Bayesian approach on SISR that produces high-resolution images along with a confidence map of reconstruction quality. In this regards, we discuss a short background of Bayesian inference in this section. After that, we define our network architecture and its modification for Bayesian approximation. We also present a faster and better approach to overcome the difficulties of estimating uncertainty in SISR applications. In the end, we discuss metrics to measure the quality of uncertainty.

#### 3.1. Bayesian Inference

We estimate a probabilistic function  $F_W(I) : I_{LR} \rightarrow I_{HR}$  from a training set  $D = \{\tilde{I}_{LR}, \tilde{I}_{HR}\}$  where  $\tilde{I}_{LR} = \{\tilde{I}_{LR_1}, \dots, \tilde{I}_{LR_n}\}$  are LR image set and its corresponding HR image set  $\tilde{I}_{HR} = \{\tilde{I}_{HR_1}, \dots, \tilde{I}_{HR_n}\}$ . This function is approximated to generate most likely high-resolution image  $I'_{HR}$  from a low-resolution test image  $I'_{LR}$ . So the probabilistic estimation of HR test image is described as

$$p(I'_{HR}|I'_{LR}, D) = \int p(I'_{HR}|I'_{LR}, W)p(W|D)dW \quad (1)$$

where  $W$  is weight parameters of a function  $F_W(I)$ . We use variational inference to approximate Bayesian modeling. Most common approach is to learn approximate distribution of weights  $q_\theta(w)$  by minimizing the KullbackLeibler divergence  $KL(q_\theta(w) \parallel p(W|D))$ . This yields approximate distribution

$$q(I'_{HR}|I'_{LR}, D) = \int p(I'_{HR}|I'_{LR}, w)q_\theta(w)dw \quad (2)$$

In a batch-normalized neural network for Bayesian uncertainty estimation, model parameters are  $W_L, \gamma_L, \beta_L, \mu_L, \sigma^2_L$ . Here  $\theta = \{W_L, \gamma_L, \beta_L\}$  is learnable model weight parameters and  $w = \{\mu_L, \sigma^2_L\}$  are stochastic parameters which are mean and variance of each layer.  $q_\theta(w)$  is a joint distribution of weights and stochastic parameters  $w$ .  $w_i$  is mean and variance of  $i$ 's sample and it need to be Independent and identically distributed random variables.

#### 3.2. Network Architecture

In this paper, we use very deep super-resolution (VDSR) network [18] as a base architecture for an experimental pur-

pose to analyze uncertainty. Our method is a generalized approach, and it can be extended to any other super-resolution network. We have used batch-normalization to measure uncertainty, but VDSR paper has not used batch-normalization (BN). So we introduce some changes in the main architecture. Our VDSR architecture has batch-normalization layer after each convolutional layer except the last layer, and no bias is used as batch-normalization normalizes the output. BN blocks are followed by convolution and ReLU non-linearity.

#### 3.3. Bayesian VDSR for Uncertainty Estimation

We use batch-normalization [13] to estimate the uncertainty of super-resolution network. It is commonly used in deep networks to overcome the problem known as internal covariate shift. Random batch members are selected to estimate mini-batch statistics for training. We use this stochasticity to approximate Bayesian inference. This allows us to make a meaningful estimate of uncertainty, and it is termed as Monte Carlo Batch Normalization (MCBN) [33]. Generally running batch mean and batch variance are estimated in each batch normalization layer during training, but we use batch mean and variance both during training and testing. We have learnable model parameters which are optimized using gradient back-propagation during training and stochastic parameters like batch mean and variances help to generate MC samples from the posterior distribution of the model. We feed-forward a test image along with different training batch for multiple times, and due to stochasticity of batches, it creates various reconstructed HR images. We take mean of those MC samples to get estimated reconstruction and variance for getting uncertainty map.

#### 3.4. Faster approach

The main drawback of Bayesian uncertainty estimation in the batch-normalized neural network is that we need to process test image with different random batches to generate MC samples and computation time increases exponentially with the increase of the number of samples in a single batch or spatial dimension of the batch. Another challenge is that in the case of SISR, test image size varies from thousands to millions of pixel. We can not make higher spatial batch size during training as it takes longer computation time. We train our model using small batch size due to the computational constraint. So we have to break larger images during testing for batch processing, and it can create a patchy effect in images. Due to this, we propose a different approach to generate MC samples in a single batch. After training, we estimate stochastic parameters  $w_L$  of each layer using different random training batches as shown in Algorithm 1. We use the same batch shape during training and stochastic parameter estimation. These parameters in each batch-normalization layer are estimated for a batch,

---

**Input:** training image set  $I$

**Output:** layer-wise batch mean and variance set  $\hat{w}_L^T = \{\mu_L^T, \sigma^2_L\}$  of trained network. Where  $L$  is layer no and  $T$  is maximum number of MC samples required.

**Training SR Network:**

**for** total iterations **do**

**forall** images of  $I$  **do**

$b$  number of  $n \times n$  random crop;  
        train();

**end**

**end**

$\hat{w}_L^T$  **estimation:**

**forall** images of  $I$  **do**

    random crop;  $\backslash \backslash$  crop size =  $n \times n$  ;  
    concat patches  $\rightarrow B \backslash \backslash T$  decides patch/image;

**end**

shuffle( $B$ );

batchsize =  $b$ ;  $\backslash \backslash$  same as training;

**forall** batches of  $B$  **do**

    forward pass;  
    estimate  $\hat{w}_L^T$  ;

**end**

---

**Algorithm 1:** Layer-wise batch mean and variance estimation for single shot MC samples generation

and like this, we create several stochastic parameters set for various batches. These stochastic parameters will be used during testing for generating MC samples. One stochastic parameter set generates one MC sample. During testing, we concatenate the same test image based on the required number of MC samples and in batch-normalization layer we normalize each image separately using different stochastic parameters as shown in Algorithm 2. Due to this, it produces various HR image as an MC samples which come from a posterior distribution learned from the training dataset.

---

**Input:** test image  $I_{LR}$ , number of MC samples  $T$ , batch mean and variance of layer  $L$  and inference  $\hat{w}_L^T = \mu_L^T, \sigma^2_L$

**Output:** image mean prediction  $\hat{I}_{HR}$ , predictive image uncertainty  $\sigma^2$

concat  $I_{LR}$  for  $T$  times ( $I^T_{LR}$ );

$I^T_{HR} = F_w(I^T_{LR}, \hat{w}_L^T)$ ;

$\hat{I}_{HR} = \text{mean}(I^T_{HR})$ ;

$\sigma^2 = \text{var}(I^T_{HR})$ ;

---

**Algorithm 2:** MCBN algorithm for SISR uncertainty

### 3.5. Uncertainty Quality Metrics

We evaluate quality of uncertainty using two standard statistical metrics, Predictive Log Likelihood (PLL) and Continuous Ranked Probability Score (CRPS).

**Predictive Log Likelihood (PLL):** Predictive Log Likelihood is a widely accepted metric for measuring the quality of uncertainty [4, 11, 33, 8]. For a probabilistic model  $F_w(x | D)$ , PLL of an LR image  $i_{LR}$  and HR image  $i_{HR}$  is defined as:

$$PLL(F_w(x | D), (i_{LR}, i_{HR})) = \log p(i_{HR} | F_w(x | D)) \quad (3)$$

$p(i_{HR} | F_w(x | D))$  is a predictive probability distribution function of  $i_{HR}$  for an input  $i_{LR}$ . There is no bound of PLL and it is maximized for perfect prediction of HR image without any variance. Main property of this metric is that it does not make any assumptions about distribution but it is criticized for have effect of outlier on score [28].

**Continuous Ranked Probability Score (CRPS):** Continuous Ranked Probability Score [10] is generally used to estimate respective accuracy of two probabilistic models. It generalizes mean absolute error for probabilistic estimation. CRPS is defined as

$$CRPS(F_w(i_{LR} | D), i_{HR}) = \int_{-\infty}^{\infty} (F(y) - \mathbf{1}(y - i_{HR}))^2 dy \quad (4)$$

where  $F(y)$  is predictive cumulative distribution function, and  $\mathbf{1}$  is the Heaviside step function. The value of  $\mathbf{1}(y - i_{HR})$  is 1 if  $y - i_{HR} \geq 0$  and 0 otherwise. There is no upper bound of crps. Perfect prediction with no variance receives a CRPS of 0.

## 4. Experimental Results & Discussions

In this section, we discuss the datasets used in experimental purpose and training methodology. We also address the effect of the number of MC samples on performance and compare our faster MC sample generation approach with standard BN uncertainty estimation. In the end, we present our understanding of model uncertainty for SISR applications.

### 4.1. Datasets

We use DIV2K [2, 35], a high-resolution, high-quality dataset for training purpose. Total 800 training images optimize trainable parameters of the SR network, and 100 validation images are to select the best parameter settings for testing. We analyze the network performance using five standard benchmark testing dataset namely Set5 [3], Set14 [40], BSD100 [25], Urban100 [12], and Manga109 [26]. We have also experimented on satellite images downloaded from [1] and histopathological images from MoNuSeg challenge dataset [21].



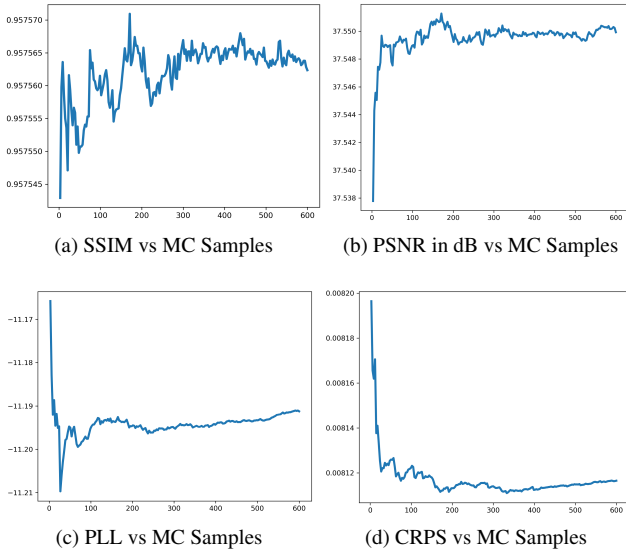


Figure 2: The plot shows estimated values on 'Set5' dataset for a scale factor  $\times 8$  and MC samples vary from minimum 3 samples to 600 samples.

## 4.2. Training Details

We randomly extract 16 patches of size  $64 \times 64$  from each HR and bicubic interpolated LR image during training for a batch update. We augment the patches by horizontal flip, vertical flip, and 90-degree rotation and randomly choose each augmentation with 50% probability. We normalize each input into  $[0, 1]$  before feeding to the network. We train each model for 1,000 iterations which is equivalent to 0.8 million batch update. To ensure better convergence, we use trained model of scale factor  $\times 2$  as initialization for other scale factors. We use Xavier initialization [9] for initializing model of scaling factor 2. We train our model with PyTorch framework and update weights with Adam optimizer [20]. The learning rate is initialized to  $10^{-4}$  and reduced to half after every 400 iterations. We use mean-squared error to optimize model parameters. We extract  $64 \times 64$  patches from high variance regions of validation images to choose the best model for testing. During testing, we clip the output between  $[0, 1]$  and map into an 8-bit unsigned integer format. For a fair comparison, we remove boundary pixels of each test image based on the scaling factor for image quality evaluation as described in vdsr paper [18].

## 4.3. Performance Analysis

### 4.3.1 Number of MC Samples

We get a better estimate of uncertainty and reconstruction with the increase of the number of MC samples, but it also increases the inference time. So proper choice of the num-

Monte Carlo Samples	Bayesian VDSR	Faster Implementation
5	14.28	1.0
10	33.48	1.97
15	52.67	2.96

Table 1: All the values correspond to 'face' image of size  $276 \times 276$  from 'Set14' dataset.

ber of MC samples required for the task from this trade-off. The minimum number of MC samples should be capable enough to give a better reconstruction than batch-normalization without stochastic mean-variance and should also provide a stable uncertainty map. In the figure 2, we observe the changes of reconstruction and uncertainty quality against changes in the number of MC samples for 'Set5' dataset. The plot shows that SSIM and PSNR index increases with the increase of MC samples and later it settles to some stable values. In the case of PLL and CRPS, it converges to some stable value after initial unstable conditions. In our experiments, We use 5, 15, and 25 MC samples for testing.

### 4.3.2 Fast MC Sample Generation

We benchmark our faster approach with standard batch-normalized (BN) uncertainty estimation. The time required for generating MC samples in standard BN uncertainty [33] mainly depends on the size of the image in the dataset and the number of MC samples. We overcome these two difficulties. Our approach is much faster than conventional as shown in Table 1. We consider 5 MC sample generation for an image using our method as a baseline and other values in the table exhibits how many times more GPU time required for inference. Our approach takes 14.28 times lesser execution time to generate 5 samples for an image of size  $276 \times 276$ .

### 4.3.3 Image Quality Analysis

We used structural similarity (SSIM) [37] and peak signal-to-noise ratio (PSNR) metrics to measure the reconstruction quality. Table 2 shows the performance of Bayesian VDSR for different Monte Carlo samples. We observe an improvement of image quality with the increase of MC samples and it saturates gradually. In Table 3, we also compared our bayesian VDSR and batch-normalized (BN) VDSR with standard deep learning based approaches like SRCNN [5], VDSR [18]. Our training dataset, training procedure and no bias approach are different from VDSR paper. So we put our VDSR implementation in the table for fair comparison. Bayesian VDSR gives a minor improvement over BN-VDSR. But along with this, uncertainty map comes free,

Scaling Factor		$\times 2$			$\times 4$			$\times 8$		
MC Samples		5	15	25	5	15	25	5	15	25
Set5	SSIM	0.957530	0.957559	<b>0.957562</b>	0.884546	<b>0.884700</b>	0.884685	0.732343	<b>0.732507</b>	0.732317
	PSNR	37.5404	37.5440	<b>37.5472</b>	31.4436	<b>31.4456</b>	31.4443	26.0340	<b>26.0409</b>	26.0391
	PLL	<b>-11.175</b>	-11.187	-11.184	<b>-41.361</b>	-41.392	-41.434	-157.733	<b>-157.559</b>	-157.656
	CRPS	0.008191	0.008162	<b>0.008157</b>	0.015771	0.015711	<b>0.015693</b>	0.032864	0.032843	<b>0.032823</b>
Set14	SSIM	0.912049	0.912211	<b>0.912232</b>	0.768863	0.768996	<b>0.769027</b>	0.615298	0.615382	<b>0.615404</b>
	PSNR	33.0858	33.1049	<b>33.1096</b>	28.0506	28.0637	<b>28.0640</b>	24.2733	24.2783	<b>24.2816</b>
	PLL	-91.007	-90.892	<b>-90.767</b>	-252.040	<b>-250.839</b>	-250.943	-568.926	-568.596	<b>-568.283</b>
	CRPS	0.014960	0.014879	<b>0.014857</b>	0.026334	0.026215	<b>0.026199</b>	0.040444	<b>0.040339</b>	0.040343
BSD100	SSIM	0.894965	0.895038	<b>0.895048</b>	0.725807	0.725903	<b>0.725940</b>	0.580028	<b>0.580055</b>	0.580051
	PSNR	31.9119	31.9164	<b>31.9175</b>	27.2973	27.2997	<b>27.3012</b>	24.4825	24.4842	<b>24.4845</b>
	PLL	-74.233	-74.226	<b>-74.217</b>	-195.734	-195.736	<b>-195.730</b>	-346.074	<b>-345.979</b>	-345.981
	CRPS	0.016905	0.016859	<b>0.016851</b>	0.028345	0.028274	<b>0.028260</b>	0.039483	0.039417	<b>0.039400</b>
Urban100	SSIM	0.916389	0.916472	<b>0.916480</b>	0.757138	<b>0.757218</b>	0.757180	0.576144	<b>0.576194</b>	0.576157
	PSNR	31.1339	31.1442	<b>31.1457</b>	25.3401	<b>25.3423</b>	25.3417	<b>21.8184</b>	21.8180	21.8176
	PLL	-472.235	-469.221	<b>-468.409</b>	-1553.83	-1547.44	<b>-1545.33</b>	-3148.43	-3140.58	<b>-3138.79</b>
	CRPS	0.017461	0.017389	<b>0.017373</b>	0.033442	0.033353	<b>0.033327</b>	0.052008	0.051922	<b>0.051906</b>
Manga109	SSIM	0.973192	0.973270	<b>0.973291</b>	0.887527	0.887976	<b>0.888069</b>	0.726837	0.727066	<b>0.727109</b>
	PSNR	37.5643	37.5966	<b>37.6036</b>	29.1394	29.1608	<b>29.1634</b>	23.3169	23.3217	<b>23.3223</b>
	PLL	-127.31	-127.00	<b>-126.71</b>	-796.85	-791.92	<b>-790.55</b>	-2640.54	-2634.91	<b>-2632.31</b>
	CRPS	0.007538	0.007450	<b>0.007427</b>	0.017915	0.017773	<b>0.017740</b>	0.036155	0.036030	<b>0.035989</b>

Table 2: Average SSIM, PSNR, PLL and CRPS for different scale factor and MC samples on 5 standard dataset.

Dataset	Scale	Bicubic	A+	SRCNN	VDSR	VDSR (Our Implementation)	BN VDSR (Ours)	Bayesian VDSR (Ours)
Set5	$\times 2$	33.65 / 0.930	36.54 / 0.954	36.65 / 0.954	37.53 / 0.958	37.49 / 0.957	37.54 / 0.957	<b>37.55 / 0.958</b>
	$\times 4$	28.42 / 0.810	30.30 / 0.859	30.49 / 0.862	31.35 / 0.882	31.32 / 0.882	31.45 / 0.884	<b>31.45 / 0.885</b>
	$\times 8$	24.39 / 0.657	25.52 / 0.692	25.33 / 0.689	25.72 / 0.711	26.00 / 0.729	<b>26.07 / 0.732</b>	26.04 / <b>0.733</b>
Set14	$\times 2$	30.34 / 0.870	32.40 / 0.906	32.29 / 0.903	32.97 / 0.913	33.03 / 0.912	33.08 / 0.912	<b>33.11 / 0.912</b>
	$\times 4$	26.10 / 0.704	27.43 / 0.752	27.61 / 0.754	28.03 / 0.770	28.02 / 0.767	<b>28.07 / 0.768</b>	28.06 / <b>0.769</b>
	$\times 8$	23.19 / 0.568	23.98 / 0.597	23.85 / 0.593	24.21 / 0.609	24.26 / 0.613	<b>24.32 / 0.615</b>	24.28 / <b>0.615</b>
BSD100	$\times 2$	29.56 / 0.844	31.22 / 0.887	31.36 / 0.888	31.90 / 0.896	31.88 / 0.895	31.91 / 0.895	<b>31.92 / 0.895</b>
	$\times 4$	25.96 / 0.669	26.82 / 0.710	26.91 / 0.712	27.29 / 0.726	27.27 / 0.724	27.30 / 0.725	<b>27.30 / 0.726</b>
	$\times 8$	23.67 / 0.547	24.20 / 0.568	24.13 / 0.565	24.37 / 0.576	24.46 / 0.579	<b>24.49 / 0.579</b>	24.48 / <b>0.580</b>
Urban100	$\times 2$	26.88 / 0.841	29.23 / 0.894	29.52 / 0.895	30.77 / 0.914	31.05 / 0.916	<b>31.15 / 0.917</b>	<b>31.15 / 0.916</b>
	$\times 4$	23.15 / 0.659	24.34 / 0.720	24.53 / 0.724	25.18 / 0.753	25.27 / 0.754	<b>25.35 / 0.756</b>	25.34 / <b>0.757</b>
	$\times 8$	20.74 / 0.515	21.37 / 0.545	21.29 / 0.543	21.54 / 0.560	21.77 / 0.574	<b>21.83 / 0.576</b>	21.82 / <b>0.576</b>
Manga109	$\times 2$	30.84 / 0.935	35.33 / 0.967	35.72 / 0.968	37.16 / 0.974	37.36 / 0.973	37.46 / 0.973	<b>37.60 / 0.973</b>
	$\times 4$	24.92 / 0.789	27.02 / 0.850	27.66 / 0.858	28.82 / 0.886	28.98 / 0.885	<b>29.20 / 0.888</b>	29.16 / <b>0.888</b>
	$\times 8$	21.47 / 0.649	22.39 / 0.680	22.37 / 0.682	22.83 / 0.707	23.23 / 0.723	<b>23.35 / 0.728</b>	23.32 / 0.727

Table 3: Comparison table of Bayesian VDSR with other benchmarked results. Average PSNR / SSIM values for scaling factor  $\times 2$ ,  $\times 4$ ,  $\times 8$

and it contributes a significant boost in deep learning based super-resolution task.

#### 4.4. Understanding Model Uncertainty

The Table 2 shows two standard uncertainty quality metrics PLL and CRPS for measuring uncertainty quality using different MC samples. We observe the value of PLL and CRPS are getting better (more stable) with the increase of MC samples due to the availability of larger samples it can

estimate better mean and variance. Model uncertainty increases with the increase of scaling factor due to the higher shift of mean from actual value and higher variance in MC samples.

In Figure 3 shows 3 different images from a standard testing dataset and its reconstruction from LR image with the different scaling factor. Along with this it also shows uncertainty in reconstruction. In the first image, if we look on the English letters, we can see higher uncertainty in bor-

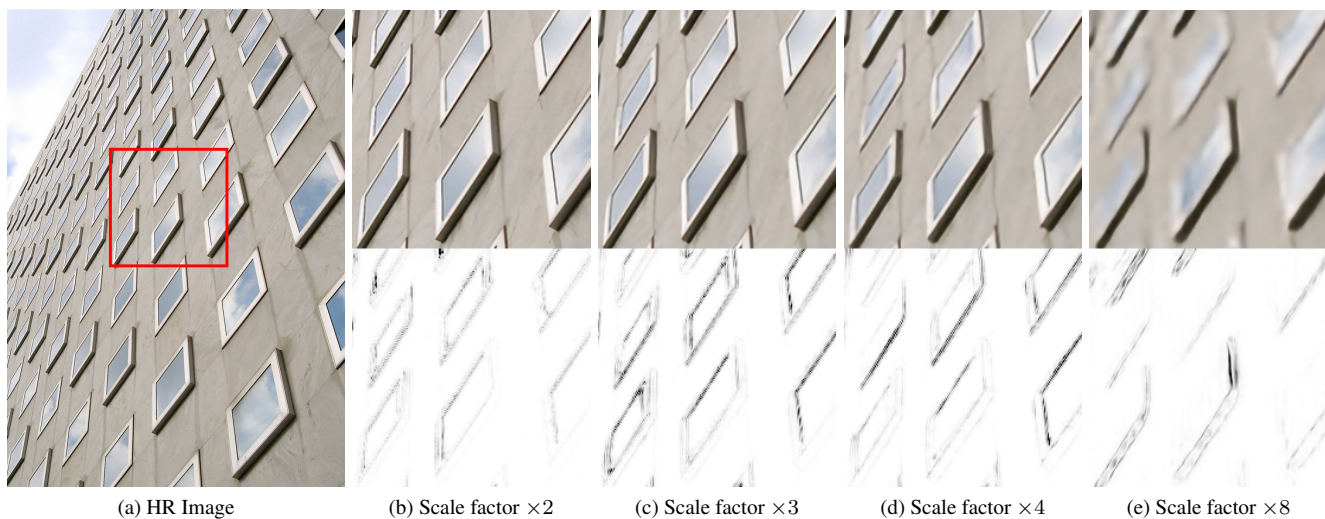
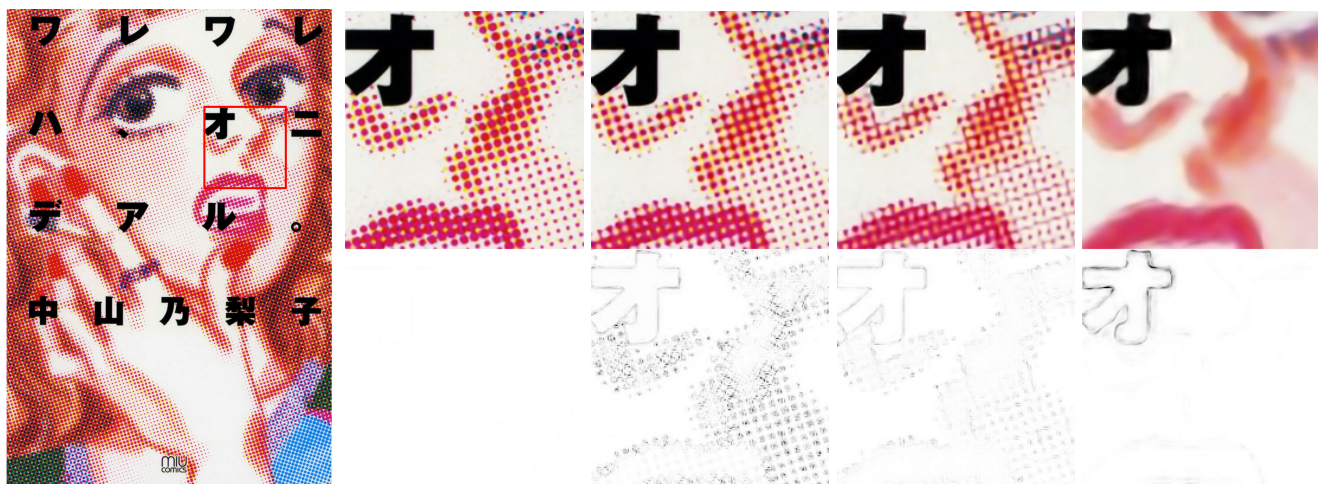
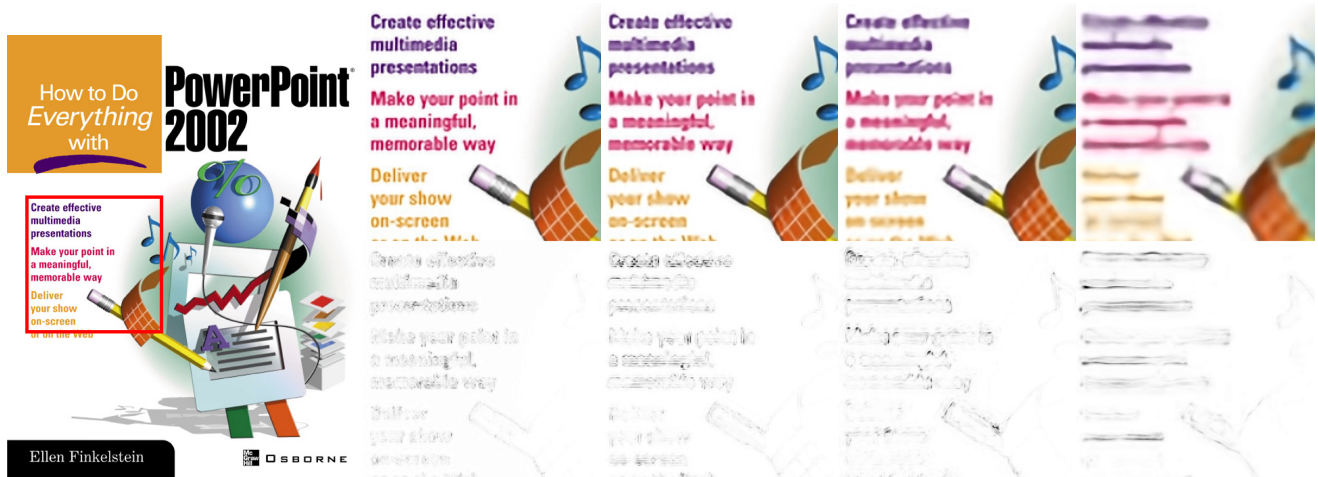


Figure 3: Figure shows reconstructed image and uncertainty map with different scaling factor. First two image is from 'Manga109' dataset and last one is from 'Urban100' dataset.



der of each letter for scaling factor  $\times 2$ , and as scaling factor increases it becomes difficult to reconstruct the characters perfectly for a DL models and uncertainty increases as we can see for scaling factor  $\times 8$ , model shows uncertainty all over the characters. In the second image set of figure 3, the reconstructed image with scaling factor  $\times 2$  does not show any uncertainty. But we observe there is uncertainty in the boundary of Japanese character and it increases gradually with the increase of scaling factor. Uncertainty is maximum for scaling factor  $\times 8$  as we can also see visually that sharp boundary in that character has been deformed in the reconstructed image. But in case of dotted texture in that image shows higher uncertainty for scaling factor  $\times 3$  and there is no uncertainty for scaling factor  $\times 2$  and  $\times 8$ . It is due to perfect reconstruction for scaling factor  $\times 2$  but for scaling factor  $\times 8$ , these texture has completely been abolished in original low LR image due to high downsampling, and the dotted region becomes continuous, and model upsampled that continuous texture. The last image set of Figure 3 shows the uncertainty in the edges of windows, and it increases with the increase of downsampling factor. In our understanding, we observe that if some texture is present in LR image and it is not reconstructed properly in HR image, those regions show higher uncertainty in the reconstruction. Mainly ambiguous regions, object boundaries, sharp regions or any deformed reconstruction generally receive higher uncertainty. This is very much helpful to further process those images for other computer vision task. Features coming from those uncertain regions in other computer vision task can be assigned lower importance, and it may improve performance.

For qualitative evaluation, we compare the average uncertainty with the quality of reconstruction. In Figure 4, we use PSNR and perceptual loss [14] to measure the quality of reconstruction. We use features of *relu2\_2*, *relu3\_3*, and *relu4\_3* layer from popular VGG16 [31] model to calculate perceptual loss between HR image and reconstructed image. Perceptual loss increases with the increase of deformation in the reconstructed image and PSNR decreases with the increase of pixel-wise loss. We observe a strong relationship between uncertainty and image quality. PSNR decreases and perceptual loss increases with the rise in uncertainty.

## 5. Conclusion

In this article, we introduced a Bayesian approach to estimate uncertainty in batch normalized super-resolution network. Stochastic batch-normalization used during test time to generate multiple Monte Carlo samples and those samples are used to estimate uncertainty. We also propose a faster approach to produce Monte Carlo samples and measure uncertainty quality using standard statistical metrics. Our method is a generalized approach, and it can be applied to any image reconstruction techniques. We show Bayesian

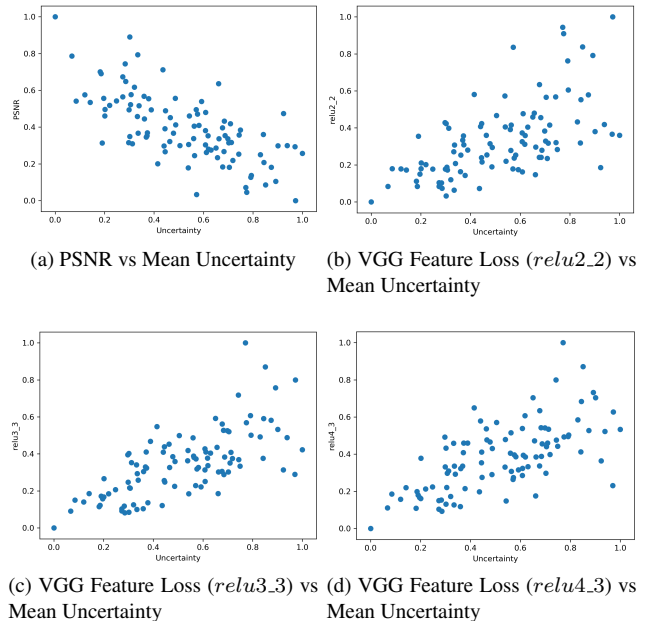


Figure 4: All the points in the plot are reconstructed images from *BSD100* dataset for a scale factor  $\times 2$  using 50 MC samples. All the axis values are normalized between  $[0, 1]$ .

uncertainty provides the reliable measure of model uncertainty in SISR. We believe that uncertainty in image super-resolution will improve the trustability of reconstructed output for deployment in the high-risk task.

## References

- [1] Open Data Program. <https://www.digitalglobe.com/ecosystem/open-data/>. Accessed: 2019-03-01. 2, 4
- [2] E. Agustsson and R. Timofte. Ntire 2017 challenge on single image super-resolution: Dataset and study. In *Proceedings of the IEEE Conference on Computer Vision and Pattern Recognition Workshops*, pages 126–135, 2017. 4
- [3] M. Bevilacqua, A. Roumy, C. Guillemot, and M. L. Alberi-Morel. Low-complexity single-image super-resolution based on nonnegative neighbor embedding. 2012. 4
- [4] T. Bui, D. Hernández-Lobato, J. Hernandez-Lobato, Y. Li, and R. Turner. Deep gaussian processes for regression using approximate expectation propagation. In *International Conference on Machine Learning*, pages 1472–1481, 2016. 4
- [5] C. Dong, C. C. Loy, K. He, and X. Tang. Image super-resolution using deep convolutional networks. *IEEE transactions on pattern analysis and machine intelligence*, 38(2):295–307, 2016. 2, 5
- [6] W. T. Freeman, T. R. Jones, and E. C. Pasztor. Example-based super-resolution. *IEEE Computer graphics and Applications*, (2):56–65, 2002. 2



- [7] Y. Gal. *Uncertainty in deep learning*. PhD thesis, PhD thesis, University of Cambridge, 2016. **2**
- [8] Y. Gal and Z. Ghahramani. Dropout as a bayesian approximation: Representing model uncertainty in deep learning. In *International Conference on Machine Learning*, pages 1050–1059, 2016. **1, 2, 4**
- [9] X. Glorot and Y. Bengio. Understanding the difficulty of training deep feedforward neural networks. In *Proceedings of the thirteenth international conference on artificial intelligence and statistics*, pages 249–256, 2010. **5**
- [10] T. Gneiting and A. E. Raftery. Strictly proper scoring rules, prediction, and estimation. *Journal of the American Statistical Association*, 102(477):359–378, 2007. **4**
- [11] J. M. Hernández-Lobato and R. Adams. Probabilistic back-propagation for scalable learning of bayesian neural networks. In *International Conference on Machine Learning*, pages 1861–1869, 2015. **4**
- [12] J.-B. Huang, A. Singh, and N. Ahuja. Single image super-resolution from transformed self-exemplars. In *Proceedings of the IEEE Conference on Computer Vision and Pattern Recognition*, pages 5197–5206, 2015. **4**
- [13] S. Ioffe and C. Szegedy. Batch normalization: Accelerating deep network training by reducing internal covariate shift. In *International Conference on Machine Learning*, pages 448–456, 2015. **1, 2, 3**
- [14] J. Johnson, A. Alahi, and L. Fei-Fei. Perceptual losses for real-time style transfer and super-resolution. In *European conference on computer vision*, pages 694–711. Springer, 2016. **8**
- [15] A. Kar, S. Phani Krishna Karri, N. Ghosh, R. Sethuraman, and D. Sheet. Fully convolutional model for variable bit length and lossy high density compression of mammograms. In *Proceedings of the IEEE Conference on Computer Vision and Pattern Recognition Workshops*, pages 2591–2594, 2018. **2**
- [16] A. Kendall, V. Badrinarayanan, and R. Cipolla. Bayesian segnet: Model uncertainty in deep convolutional encoder-decoder architectures for scene understanding. *Proceedings of the British Machine Vision Conference (BMVC)*, 2017. **1**
- [17] A. Kendall and R. Cipolla. Modelling uncertainty in deep learning for camera relocalization. In *2016 IEEE international conference on Robotics and Automation (ICRA)*, pages 4762–4769. IEEE, 2016. **1**
- [18] J. Kim, J. Kwon Lee, and K. Mu Lee. Accurate image super-resolution using very deep convolutional networks. In *Proceedings of the IEEE Conference on Computer Vision and Pattern Recognition*, pages 1646–1654, 2016. **2, 3, 5**
- [19] J. Kim, J. Kwon Lee, and K. Mu Lee. Deeply-recursive convolutional network for image super-resolution. In *Proceedings of the IEEE conference on computer vision and pattern recognition*, pages 1637–1645, 2016. **2**
- [20] D. P. Kingma and J. Ba. Adam: A method for stochastic optimization. *ICLR*, 2014. **5**
- [21] N. Kumar, R. Verma, S. Sharma, S. Bhargava, A. Vahadane, and A. Sethi. A dataset and a technique for generalized nuclear segmentation for computational pathology. *IEEE transactions on medical imaging*, 36(7):1550–1560, 2017. **2, 4**
- [22] A. Kurakin, I. Goodfellow, and S. Bengio. Adversarial examples in the physical world. *ICLR Workshop track*, 2017. **1**
- [23] W.-S. Lai, J.-B. Huang, N. Ahuja, and M.-H. Yang. Fast and accurate image super-resolution with deep laplacian pyramid networks. *IEEE transactions on pattern analysis and machine intelligence*, 2018. **2**
- [24] C. Ledig, L. Theis, F. Huszár, J. Caballero, A. Cunningham, A. Acosta, A. Aitken, A. Tejani, J. Totz, Z. Wang, et al. Photo-realistic single image super-resolution using a generative adversarial network. In *Proceedings of the IEEE conference on computer vision and pattern recognition*, pages 4681–4690, 2017. **2**
- [25] D. Martin, C. Fowlkes, D. Tal, and J. Malik. A database of human segmented natural images and its application to evaluating segmentation algorithms and measuring ecological statistics. In *Proceedings Eighth IEEE International Conference on Computer Vision. ICCV 2001*, volume 2, pages 416–423. IEEE, 2001. **4**
- [26] Y. Matsui, K. Ito, Y. Aramaki, A. Fujimoto, T. Ogawa, T. Yamasaki, and K. Aizawa. Sketch-based manga retrieval using manga109 dataset. *Multimedia Tools and Applications*, 76(20):21811–21838, 2017. **4**
- [27] A. G. Roy, S. Conjeti, N. Navab, and C. Wachinger. Inherent brain segmentation quality control from fully convnet monte carlo sampling. In *International Conference on Medical Image Computing and Computer-Assisted Intervention*, pages 664–672. Springer, 2018. **1**
- [28] R. Selten. Axiomatic characterization of the quadratic scoring rule. *Experimental Economics*, 1(1):43–61, 1998. **4**
- [29] A. Sharma, P. Kaur, A. Nigam, and A. Bhavsar. Learning to decode 7t-like mr image reconstruction from 3t mr images. In *Deep Learning in Medical Image Analysis and Multimodal Learning for Clinical Decision Support*, pages 245–253. Springer, 2018. **1**
- [30] W. Shi, J. Caballero, C. Ledig, X. Zhuang, W. Bai, K. Bhatia, A. M. S. M. de Marvao, T. Dawes, D. ORegan, and D. Rueckert. Cardiac image super-resolution with global correspondence using multi-atlas patchmatch. In *International Conference on Medical Image Computing and Computer-Assisted Intervention*, pages 9–16. Springer, 2013. **1**
- [31] K. Simonyan and A. Zisserman. Very deep convolutional networks for large-scale image recognition. *arXiv preprint arXiv:1409.1556*, 2014. **8**
- [32] N. Srivastava, G. Hinton, A. Krizhevsky, I. Sutskever, and R. Salakhutdinov. Dropout: a simple way to prevent neural networks from overfitting. *The Journal of Machine Learning Research*, 15(1):1929–1958, 2014. **1, 2**
- [33] M. Teye, H. Azizpour, and K. Smith. Bayesian uncertainty estimation for batch normalized deep networks. In *International Conference on Machine Learning*, pages 4914–4923, 2018. **1, 2, 3, 4, 5**
- [34] R. Timofte, V. De Smet, and L. Van Gool. A+: Adjusted anchored neighborhood regression for fast super-resolution. In *Asian conference on computer vision*, pages 111–126. Springer, 2014. **2**
- [35] R. Timofte, S. Gu, J. Wu, L. Van Gool, L. Zhang, M.-H. Yang, M. Haris, et al. Ntire 2018 challenge on single image

- super-resolution: Methods and results. In *The IEEE Conference on Computer Vision and Pattern Recognition (CVPR) Workshops*, June 2018. 4
- [36] T. Tong, G. Li, X. Liu, and Q. Gao. Image super-resolution using dense skip connections. In *The IEEE International Conference on Computer Vision (ICCV)*, Oct 2017. 2
- [37] Z. Wang, A. C. Bovik, H. R. Sheikh, E. P. Simoncelli, et al. Image quality assessment: from error visibility to structural similarity. *IEEE transactions on image processing*, 13(4):600–612, 2004. 5
- [38] Z. Wang, J. Chen, and S. C. Hoi. Deep learning for image super-resolution: A survey. *arXiv preprint arXiv:1902.06068*, 2019. 1
- [39] J. Yang, J. Wright, T. S. Huang, and Y. Ma. Image super-resolution via sparse representation. *IEEE transactions on image processing*, 19(11):2861–2873, 2010. 2
- [40] R. Zeyde, M. Elad, and M. Protter. On single image scale-up using sparse-representations. In *International conference on curves and surfaces*, pages 711–730. Springer, 2010. 4
- [41] H. Zhang and V. M. Patel. Densely connected pyramid dehazing network. In *The IEEE Conference on Computer Vision and Pattern Recognition (CVPR)*, June 2018. 2
- [42] K. Zhang, W. Zuo, Y. Chen, D. Meng, and L. Zhang. Beyond a gaussian denoiser: Residual learning of deep cnn for image denoising. *IEEE Transactions on Image Processing*, 26(7):3142–3155, 2017. 2
- [43] Y. Zhang, Y. Tian, Y. Kong, B. Zhong, and Y. Fu. Residual dense network for image super-resolution. In *The IEEE Conference on Computer Vision and Pattern Recognition (CVPR)*, June 2018. 2
- [44] W. W. Zou and P. C. Yuen. Very low resolution face recognition problem. *IEEE Transactions on image processing*, 21(1):327–340, 2012. 1